Dislocation-Driven CdS and CdSe Nanowire Growth

Haoyu Wu,[†,§] Fei Meng,[‡,§] Linsen Li,[‡] Song Jin,[‡,*] and Gengfeng Zheng[†,*]

[†]Laboratory of Advanced Materials, Department of Chemistry, Fudan University, Shanghai, 200433, People's Republic of China and [‡]Department of Chemistry, University of Wisconsin—Madison, 1101 University Avenue, Madison, Wisconsin 53706, United States. [§]H.W. and F.M. contributed equally to this work.

ABSTRACT

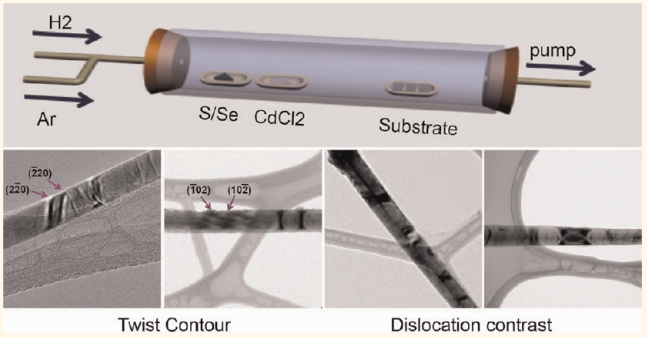

We report the synthesis of CdS and CdSe nanowires (NWs) and nanoribbons (NRs) with gold catalysts by H_2-assisted chemical vapor deposition. Nanopods and nanocones were obtained without catalysts at higher system pressure. Transmission electron microscopy (TEM) studies, including two-beam TEM and displaced-aperture dark-field TEM characterization, were used to investigate the NW growth mechanism. Dislocation contrast and twist contours have been routinely observed within the synthesized one-dimensional (1D) CdS and CdSe NWs, suggesting the operation of the dislocation-driven NW growth mechanism under our experimental conditions. The Burgers vectors of dislocations and the associated Eshelby twists were measured and quantified. We hypothesize that gold nanoparticles provide nucleation sites to initiate the growth of CdS/CdSe NWs and lead to the formation of dislocations that continue to drive and sustain 1D growth at a low supersaturation level. Our study suggests that the dislocation-driven mechanism may also contribute to the growth of other 1D nanomaterials that are commonly considered to grow *via* the vapor—liquid—solid mechanism.

KEYWORDS: nanowire · CdS · CdSe · dislocation-driven growth · Eshelby twist · chemical vapor deposition

One-dimensional (1D) semiconducting materials such as nanowires (NWs), nanotubes (NTs), and nanoribbons (NRs) are critical building blocks toward understanding fundamental properties of low-dimensional materials and realizing new device concepts and applications.[1−7] In the past decade, a variety of 1D nanomaterials have been synthesized *via* the vapor—liquid—solid (VLS),[8,9] the vapor—solid—solid (VSS),[10,11] or the solution—liquid—solid (SLS) mechanism,[12,13] where metal nanoparticles serve as the catalysts to lower the energy barrier at the catalyst—NW interface to promote 1D crystal growth. More recently, the dislocation-driven growth mechanism has been revisited and further explored to explain the catalyst-free growth of NWs and NTs,[14−16] where axial screw dislocations provide self-perpetuating growth spirals to facilitate anisotropic crystal growth. A low supersaturation level favors the dislocation-driven growth mode over the layer-by-layer (LBL) and dendritic crystal growth modes.[11,17] To date, the dislocation-driven growth mechanism has been reported/confirmed for many NW and NT materials including PbS,[14,18] PbSe,[19] ZnO,[15,20] $Co(OH)_2$,[21] FeOOH,[22] Cu,[23] and a few others[24−28] and has also been proposed to illustrate the two-dimensional growth of nanoplates.[29] Furthermore, it is suggested that the dislocation-driven growth mechanism may generally exist in a wide variety of 1D nanomaterials, such as cadmium sulfide (CdS) and cadmium selenide (CdSe) NWs, both of which possess the dislocation-prone wurtzite crystal structure yet are still usually recognized to grow *via* the VLS mechanism in modern literature.[16] Interestingly, dislocation and stacking fault defects were observed in millimeter-scale whiskers, ribbons, and platelets of CdS in the 1960s, and it was suggested that dislocations drove the initial growth of these crystals.[30]

Among the first and the most important semiconducting nanomaterials discovered,[31] CdS and CdSe have been extensively investigated due to their unique size- and structure-dependent optical and electronic properties and have found a variety of applications in solar energy conversion,[32−36] light-emitting diodes,[37−40] waveguides and lasers,[41−45] and field effect transistors.[46,47] A number of methods have been reported to synthesize CdS and CdSe nanostructures in solution or gas phase, such as solvothermal synthesis,[48,49] chemical bath deposition,[36] electrochemical deposition,[50,51] thermal evaporation,[52−55] and chemical vapor deposition (CVD).[56−60]

* Address correspondence to gfzheng@fudan.edu.cn (G.Z.); jin@chem.wisc.edu (S.J.).

Received for review March 19, 2012 and accepted April 21, 2012.

Published online April 22, 2012
10.1021/nn301194v

For the CVD growth, CdS/CdSe powder[52,53] or organometallic compounds[57] containing Cd, S, or Se are mostly used as solid precursors. It has also been reported that cadmium chloride ($CdCl_2$) and elemental sulfur,[56] or polysulfides[58] can be used as alternative reactants to provide Cd and S. In this work, we have synthesized different CdS and CdSe nanostructures using $CdCl_2$ and S/Se as precursors with a co-flown hydrogen gas (H_2) in a homemade CVD setup (Figure S1). The introduction of H_2 resulted in sufficient *in situ* conversion of S/Se into H_2S/H_2Se, which served as a more effective sulfur/selenium source.[18,61] CdS/CdSe NWs and NRs were successfully grown with uniform size distribution in the presence of a gold nanoparticle catalyst. Without the catalyst, a variety of morphologies such as nanopods and nanocones were obtained at high system pressure, while NWs were still observed to grow at relatively low pressure. Even though such results appeared to be in line with the previously reported VLS growth of 1D CdS/CdSe nanomaterials, we have observed and further rigorously characterized dislocation contrast and twist contour bands for the first time within the 1D CdS and CdSe nanomaterials synthesized with gold nanoparticle catalyst by transmission electron microscopy (TEM). These findings have further demonstrated the generality of the dislocation-driven growth mechanism, which may have long been overlooked for the growth of 1D CdS/CdSe and other nanomaterials that are commonly assumed to solely grow *via* the VLS mechanism. A comprehensive understanding of such synthesis can allow for more sophisticated design and rational control over the nanostructure growth by controlling different growth mechanisms.

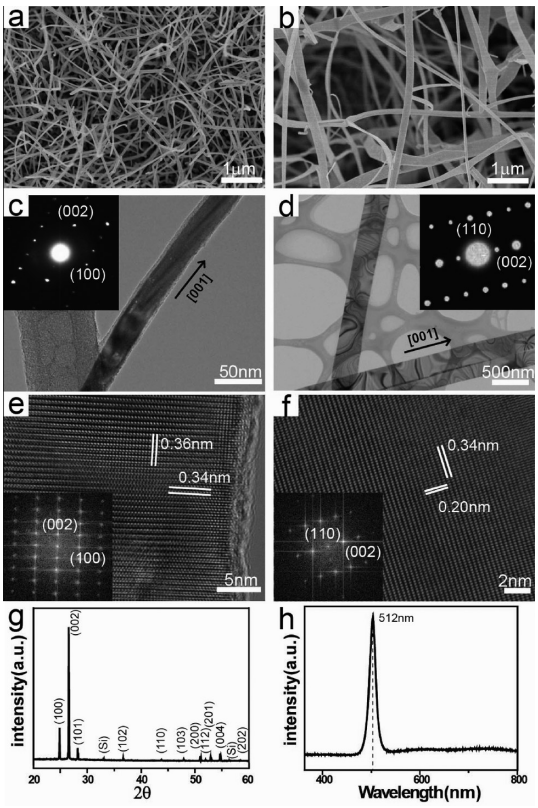

Figure 1. SEM images of synthesized (a) CdS NWs and (b) NRs. Low-magnification TEM images of (c) a CdS NW and (d) two NRs, one of which shows a potential stacking fault contrast. Insets are corresponding SAED patterns of the NW and NR in (c) and (d). (e, f) HRTEM images of the CdS NW and the NR in (c) and (d). Insets are the corresponding FFT patterns. (g) XRD pattern of as-synthesized CdS NWs. (h) Room-temperature photoluminescence spectra of CdS NWs showing a peak centered at 512 nm.

RESULTS AND DISCUSSION

A typical scanning electron microscopy (SEM) image of CdS NWs grown with gold nanoparticles at 600 °C and 40 Torr is shown in Figure 1a. These NWs had lengths of over tens of micrometers, and diameters ranged from 30 to 60 nm (Figure 1c). The diameter was uniform for each NW along the length. The selected area electron diffraction (SAED) pattern along the [010] zone axis revealed this CdS NW was a single crystal with the wurtzite structure (Figure 1c, inset). High-resolution TEM (HRTEM) images further confirmed that these CdS NWs were single crystalline (Figure 1e), with lattice fringe-resolved *d*-spacings of 0.36 and 0.34 nm, corresponding to the (100) and (002) planes in the wurtzite CdS structure. The corresponding fast Fourier transform (FFT) pattern revealed the growth direction of this NW was [001] (Figure 1e, inset). Growth directions of [010] and [110] were also observed in other as-synthesized CdS NWs, consistent with previous reports.[53,56,57] NRs were observed to grow instead of NWs at the same temperature (600 °C) and 160 Torr system pressure (Figure 1b). These NRs were typically tens of nanometers in thickness, 200 to 400 nm in width, and 30 to 50 μm in length. The widths of these NRs were uniform over their whole lengths (Figure 1b and d). The SAED pattern along the zone axis [1$\bar{1}$0] showed that these CdS NRs were single crystals with the wurtzite structure, and the NR's growth direction was along [001] (Figure 1d, f, inset) or [010]. Lattice-resolved HRTEM images revealed two *d*-spacings of 0.34 and 0.20 nm (Figure 1f), corresponding to the (002) and (110) planes of wurtzite CdS. To further analyze the composition and crystal structure of the products, X-ray diffraction (XRD) carried out directly on the as-synthesized CdS NWs (Figure 1g) or NRs confirmed that both products matched the JCPDS PDF file for wurtzite CdS [41-1049]. In addition, photoluminescence spectra taken from either CdS NWs (Figure 1h) or NRs showed only a sharp peak centered at 512 nm, in accordance with the near band gap emission of CdS (E_g = 2.4 eV).[57]

The CdSe NWs and NRs were synthesized at a higher growth temperature compared to CdS (see details in Table S1 in the Supporting Information). CdSe NWs synthesized using gold nanoparticles at 650 °C and 40 Torr had a uniform diameter distribution around 50 nm and lengths over 10 μm (Figure 2a). CdSe NRs with a

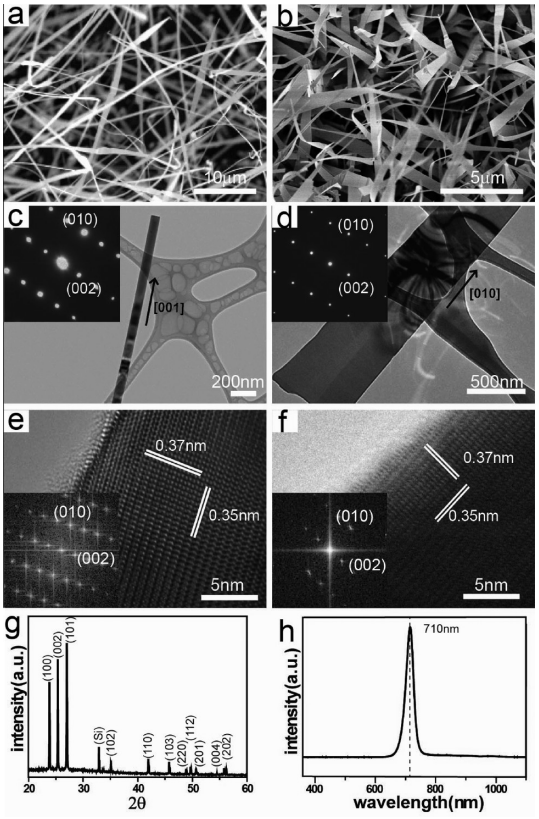

Figure 2. SEM images of as-synthesized (a) CdSe NWs and (b) NRs. Low-magnification TEM images of (c) a CdSe NW and (d) a NR. Insets are the SAED patterns of the corresponding NW and NR in (c) and (d). (e, f) HRTEM images of the CdSe NW and the NR in (c) and (d). Insets are the corresponding FFT patterns. (g) XRD pattern of synthesized CdSe NWs. (h) Room-temperature photoluminescence spectra of CdSe NWs showing a peak centered at 710 nm.

tapered morphology were obtained at 650 °C and 160 Torr (Figure 2b). The width of a typical tapered nanoribbon varied from ~500 nm at one end to 1−2 μm at the other. TEM and SAED patterns (Figure 2c, d) taken along the [100] zone axis showed that both CdSe NWs and NRs were single crystalline with a wurtzite structure. The [010] growth direction (Figure 2e, f, insets) for CdSe NWs and NRs is consistent with 1D CdSe structures synthesized by thermal evaporation.[52] Two *d*-spacings of 0.35 and 0.37 nm were observed by HRTEM, corresponding to the (002) and (010) planes of CdSe, respectively (Figure 2e, f). The XRD pattern matched the JCPDS PDF [08-0459] and further confirmed that the as-grown NWs (Figure 2g) and NRs were wurtzite CdSe. Photoluminescence emission spectra of both the CdSe NWs (Figure 2h) and NRs exhibited a single sharp peak centered at 712 nm, in accordance with the near band gap emission of CdSe (E_g = 1.7 eV).[52]

When no gold nanoparticles were used during the growth, other morphologies, including CdS nanopods (Figure 3a), CdS nanocones (Figure 3b), CdSe nanopods (Figure 3c), and CdSe nanocones (Figure 3d), were obtained under system pressures higher than

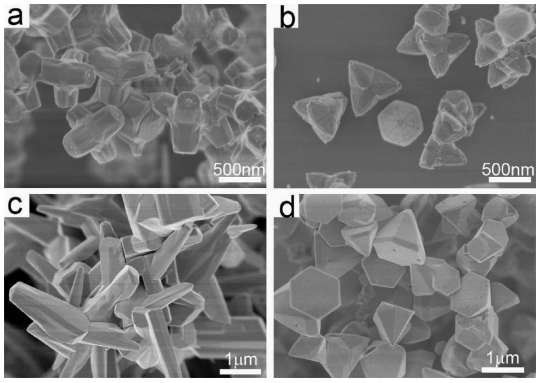

Figure 3. SEM images of (a) CdS nanopods, (b) CdS nanocones, (c) CdSe nanopods, and (d) CdSe nanocones grown without gold catalyst.

400 Torr (Table S1 in the Supporting Information). The nanocones (Figure 3b and d) were formed under relatively high supersaturation conditions, so the faceted micro- and nanocrystal growth proceeds more isotropically along various crystallographic directions based on the wurtzite structure. The nanopods (Figure 3a and c) are analogous to the CdS tetrapods from CVD[63] and solution[62] growth, which are usually formed by growing wurtzite legs epitaxially from tetrahedral zinc blende seeds nucleated initially.

Interestingly, even when the gold nanoparticle catalyst was absent, short NWs could still be grown at 600 °C under a low system pressure of 40 Torr (Figure S2). This observation suggests that the dislocation-driven growth mechanism may also exist in the growth of CdS and CdSe NWs. The reaction pressure was low in our experiments compared to most of the other reported CVD synthesis conditions;[52,56,58] therefore the precursor concentration may be in the low supersaturation regime that favors dislocation-driven crystal growth.[16]

To further understand the growth mechanism of CdSe and CdS NWs, two-beam TEM diffraction contrast imaging was carried out following the previous methods[14,15,23] to reveal any crystal defects that were present in the NWs. Screw dislocations near a nanowire core can create bending in both the real space and the reciprocal lattice, resulting in dislocation diffraction contrast along the axial direction. Such diffraction contrast is strongest when the excited diffraction spots (***g*** beams) are parallel to the Burgers vector ***b*** (***g*** ∥ ***b***) and becomes invisible when ***g*** beams perpendicular to the Burgers vector are excited (***g*** · ***b*** = 0), known as the "invisibility criterion" for the dislocation contrast.[14,15,23,64] This two-beam diffraction contrast TEM was performed for a CdSe nanowire with a [110] growth direction that displayed dislocation contrast (Figure 4d). The superposition of real space and reciprocal lattice in this CdS nanowire along [21$\bar{1}$], [31$\bar{1}$], and [001] zone axes are schematically shown in Figure 4a. The diffraction contrast was invisible when (102) spots and (103) spots were excited, respectively

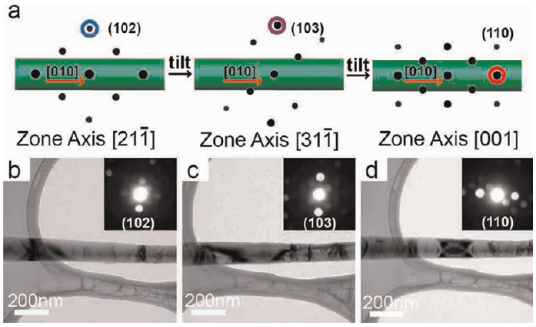

Figure 4. Diffraction contrast TEM imaging of dislocation in a CdSe NW. (a) Schematic superposition of real space and reciprocal lattice showing the process of finding *g* vectors that satisfy the "invisibility criterion". (b–d) Zero-beam TEM images with corresponding SAED patterns under strong two-beam conditions. The diffraction contrast of the screw dislocation was invisible when (102) spots and (103) spots were excited, in (b) and (c), respectively. The calculated Burgers vector direction was [120] by taking the cross product of (102) and (103). Since the (120) two-beam condition was unapproachable for this NW, the (110) spots that had a low angle with (120) spots were excited instead. The diffraction contrast was strong when (110) spots are excited in (d).

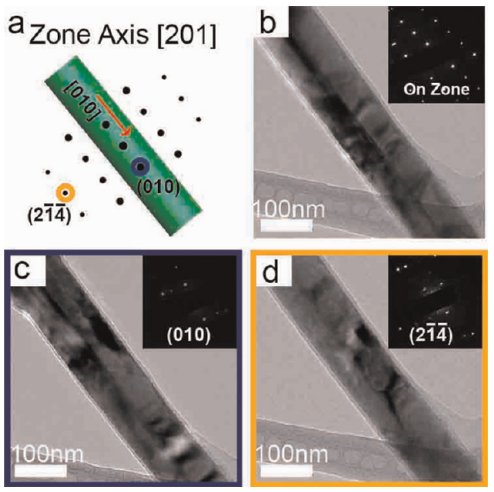

Figure 5. Diffraction contrast TEM imaging of the dislocation in a CdS NW under two-beam conditions. (a) Schematic illustration of the superposition of real space and reciprocal lattice in CdS NW along the [201] zone axis. (b) Zero-beam TEM image of a representative CdS NW on the [201] zone axis with a dislocation contrast line seen along the NW's axial direction. The growth direction of this NW was [010], and the corresponding SAED pattern is shown in the inset. (c, d) TEM images with corresponding SAED patterns under strong two-beam conditions of (010) and (2$\bar{1}\bar{4}$), respectively. The diffraction contrast was strong when the *g* vector parallel to the NW growth direction was excited (in c) and became invisible when the *g* vector perpendicular to the NW growth direction was excited (in d), suggesting the Burgers vector of this dislocation had a large screw component.

(Figure 4b, c). The Burgers vector direction of [120] was obtained by taking the cross product of (102) and (103). As the (120) two-beam condition was unattainable for this NW, the (110) spots, which had a low angle with (120) spots, were excited instead. Under this condition, the dislocation contrast was strong along the axial direction (Figure 4d). Since the NW growth axis was along the [110] direction, and the most common Burgers vector directions are ⟨110⟩, ⟨001⟩, ⟨111⟩, ⟨$\bar{1}$10⟩, and ⟨$\bar{2}$23⟩ in the wurtzite-structured crystal,[65] the dislocation along the direction of [120] in this CdSe NW is a mixed dislocation.

Similar dislocation contrast was also observed in CdS NWs under the two-beam conditions, as schematically shown in Figure 5a. For this NW along the [201] zone axis (SAED shown in Figure 5b inset), the zero-beam TEM image revealed a clear dark contrast line along the NW's axial direction (Figure 5b). When the (010) spots were excited, this dark contrast was visible (Figure 5c). When the (2$\bar{1}\bar{4}$) spots perpendicular to the NW growth direction were excited, the dark contrast along the NW axis disappeared (Figure 5d). This experiment suggested that the observed dark contrast was due to a dislocation with screw character and possibly a screw dislocation along the NW growth axis. However, in this CdS NW, the exact character cannot be conclusively determined.

Further evidence for the dislocation-driven growth can be provided by the presence of Eshelby twist,[66,67] which is the lattice rotation due to a torque around a NW axis that can relieve the stress and strain induced by axial screw dislocations.[14,15,68,69] The twist of the lattice puts different areas of the NW on or off the Bragg condition, and hence the regions satisfying the Bragg condition appear darker in the bright-field TEM image as a twist contour band, which can be further indexed *via* the complementary dark-field imaging. A representative CdSe NW with [010] growth direction imaged under bright-field TEM showed a pair of twist contour bands (indicated by the purple arrows marked with indices in Figure 6a. The origin of these contour bands could be revealed by the displaced-aperture dark-field TEM analysis. In brief, a pair of ***g*** vectors that are not parallel to the NW growth direction are selected to excite. Specifically, the ***g*** vectors orthogonal to the growth axis do not need angle correction for the Eshelby twist calculation and thus are ideal to select. In this case, the CdSe NW was first tilted to near the [201] zone axis (Figure 6a, inset); then the objective lens aperture was applied to the (10$\bar{2}$) beam (the red circle highlighted in the SAED pattern) while keeping all other diffraction spots blocked. Then only one of the bands appeared to be bright against a dark background in the displaced-aperture dark-field image (Figure 6b). Similarly, when the objective lens aperture was applied to the other diffraction spot indexed as ($\bar{1}$02) planes (the yellow circle highlighted in the SAED pattern), the other band appeared to be bright in the displaced-aperture dark-field image (Figure 6c). This experiment indicated this pair of dark bands was twist contoured. On the other hand, another pair of bands on the right in Figure 6a was found to be bend

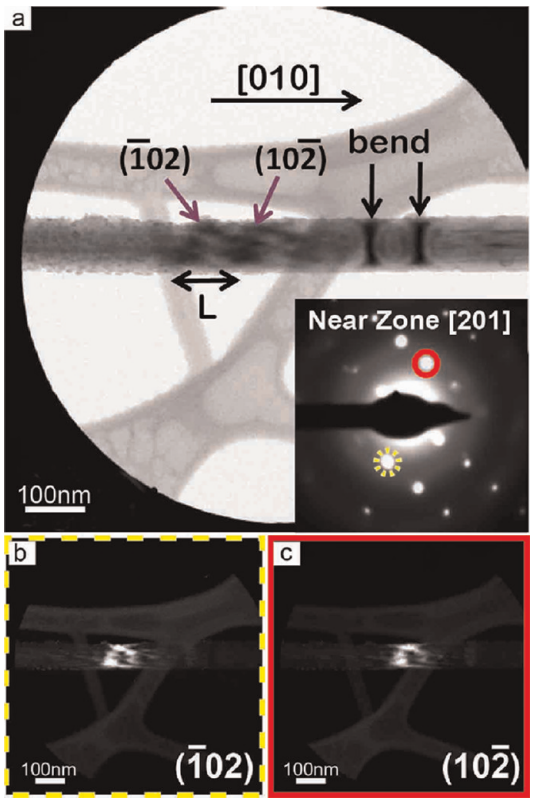

Figure 6. Twist contour analysis of a representative CdSe NW. (a) Bright-field TEM image of a single CdSe NW (radius ~40 nm) tilted to near the [201] zone axis. Two purple arrows marked with indices indicate the positions of two twist contour bands, and black arrows on the right indicate the position of two bend contours. The spacing between the two twist contours (*L*) was ~85 nm. Inset is the SAED pattern near zone axis [201]. (b, c) Dark-field TEM images of this CdSe NW in (a), when an objective aperture was sequentially applied to the two diffraction spots labeled (10$\bar{2}$) and ($\bar{1}$02), respectively. The corresponding twist contours appear as bright contrast against a dark background.

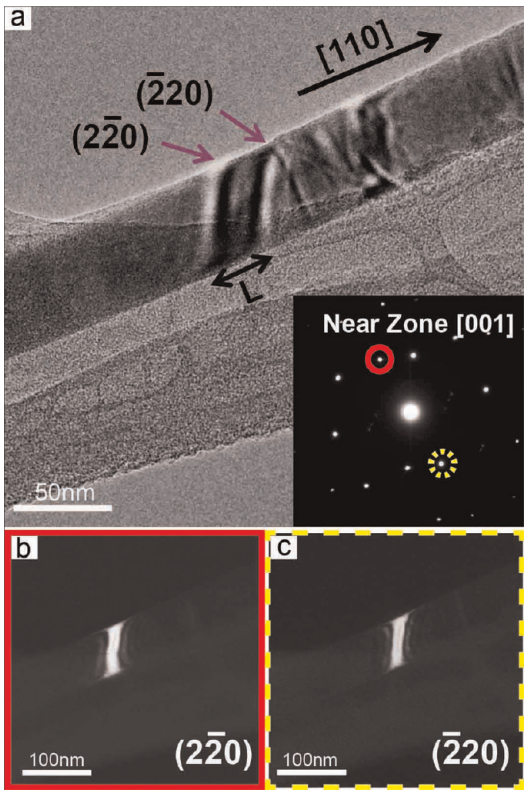

Figure 7. Twist contour analysis of a CdS NW. (a) Bright-field TEM image of a single CdS NW (radius ~25 nm) tilted to near the [001] zone axis. Two purple arrows marked with indices indicate the positions of two twist contour bands. The spacing between the two twist contours (*L*) was ~30 nm. Inset is the SAED pattern near zone axis [001]. (b, c) Dark-field TEM images of twist contour in (a), when an objective aperture was sequentially applied to the two diffraction spots labeled (2$\bar{2}$0) and ($\bar{2}$20), respectively. The corresponding twist contours appear as bright contrast against a dark background.

contoured, which responded to the excitation of ***g*** vectors that were parallel to the growth direction (see Figure S3 in the Supporting Information). The twist angle (α) for this CdSe NW was then calculated using the following equation:[23]

$$\alpha = \frac{\lambda}{2L} \left| \frac{\boldsymbol{g}_+ - \boldsymbol{g}_-}{\sin\theta} \right|$$

where λ is the wavelength of the electron (2.508 pm under 200 kV accelerating voltage), $\boldsymbol{g}_+$ and $\boldsymbol{g}_-$ are the corresponding reciprocal lattice vectors [(10$\bar{2}$) and ($\bar{1}$02)], *L* is the spacing between the two twist contour bands, and θ is the angle between $\pm\boldsymbol{g}$ and the growth direction (70° in this case). The twist angle was 7°/μm for this CdSe NW. Using the relationship between the twist angle (α) and the Burgers vector,[14]

$$\alpha = \frac{b}{\pi r^2}$$

where *r* represents the NW radius, the Burgers vector magnitude was calculated to be 0.6 nm. This value of Burgers vector magnitude is reasonable, as one-half of the (010) spacing (the NW growth direction and thus the screw component direction of the dislocations) is 0.215 nm for wurtzite CdSe. Another CdSe NW with a twist angle of 14°/μm is shown in Figure S4.

A similar twist contour analysis was carried out on CdS NWs. In a representative zero-beam bright-field TEM image, the twist contour bands were also observed (Figure 7a). As the growth direction of this selected CdS NW was [110], the NW was first tilted near the [001] zone axis, and then the two diffraction spots indexed as (2$\bar{2}$0) and ($\bar{2}$20) were sequentially selected for excitation and imaging (Figure 7a, inset). The two contrast bands on the left corresponding to these two diffraction spots (indicated by the two purple arrows marked with indices in Figure 7a) were sequentially visible in the displaced-aperture dark-field TEM image (Figure 7b, c), confirming that these two bands were twist contours. A twist angle of 13.2°/μm and the corresponding Burgers vector magnitude of 0.8 nm were calculated from this selected CdS NW (θ in this case is 90°). This magnitude is also reasonable, as one-half of the (110) spacing (the NW growth direction

and thus the screw component direction of the dislocations) is 0.37 nm for wurtzite CdS.

The evidence of dislocation contrast TEM and twist contour analysis presented above clearly showed that dislocation-driven NW growth had occurred during the CVD growth of CdS and CdSe NWs, even when gold nanoparticle catalysts were employed for the synthesis. We hypothesize that both the VLS growth and the dislocation-driven growth mechanism can coexist in the growth of 1D CdS and CdSe NWs. It was clear that short NWs can be produced on the surface of clean silicon substrates without the presence of gold nanoparticle catalysts (Figure S2), while the low yield and slow growth rate of these NWs may result from the low density of nucleation sites and large mismatch of lattice constants between the Si/SiO_2 substrate and CdS or CdSe. Other nanostructures, such as nanopods and nanocones, can form under higher temperature and pressures, where the supersaturation levels are high so that the LBL growth and other crystal growth modes take effect and result in more isotropic faceted microcrystals,[14,15,19] in addition to the branching observed in nanopods due to the zinc blende to wurtzite transition. The addition of gold nanoparticles as catalysts promotes the nanostructure growth with high yield by creating numerous nucleation sites, and thus facile and fast 1D crystal growth is initiated. However, the addition of gold impurities and the fast and disordered crystal growth could potentially lead to the generation of dislocation sites that further facilitate the crystal growth process, which might become more responsible for the subsequent NW growth at the low supersaturation level. This is consistent with previous reports of epitaxial growth of CdS and CdSe NWs on GaAs substrate[70] or mica substrates,[54] both of which could also provide dislocation sites for nucleation. The fact that dislocation-driven NW growth could happen to CdS and CdSe NW growth when gold nanoparticles were used is also analogous to the report of bismuth-catalyzed PbSe NW growth, which shows screw dislocation.[19] At relatively low temperatures and low pressures, the supersaturation level is low, so the dislocation-driven growth is more favored and plays a more important role to sustain the 1D growth. This hypothesis has been confirmed by TEM analysis from many (>30) of our CdS and CdSe 1D nanostructures in this study. Although dislocation contrast and twist contours have been directly observed only for CdS and CdSe NWs, other structural imperfections including voids, tubular structures, and potentially stacking faults have been commonly observed in CdS and CdSe NWs and NRs synthesized in our experiments (see Figures S5–S7 in the Supporting Information). Spontaneous formation of voids or tubular structures inside a NW alleviates stress and strain of screw-dislocation with large Burgers vectors.[15,23] These voids and nanotubes resulting from the release of strain energy during the axial growth, along with the twist contours, provide strong evidence for the operation of a dislocation-driven 1D growth mechanism during the formation of these nanostructures.

CONCLUSIONS

In summary, we report the synthesis of CdS/CdSe nanowires and nanoribbons by a H_2-assisted CVD process. Other nanostructures such as nanopods and nanocones were obtained in the absence of gold nanoparticles. Axial dislocation contrast, twist contours, voids, and tubular structures were often observed in these 1D CdS and CdSe nanostructures. This evidence strongly suggests that dislocation-driven NW growth does occur under our growth conditions of these CdS and CdSe nanomaterials, even when gold nanoparticle catalysts are used. We hypothesize that gold nanoparticles provide nucleation sites to promote and initiate the growth of CdS/CdSe NWs, which further leads to dislocation sites that are responsible for the dislocation-driven growth. At a low supersaturation level, these dislocation sites continue to drive and sustain the 1D growth. Our study suggests that the dislocation-driven growth may contribute to other 1D nanomaterials that are commonly considered to grow solely *via* the VLS mechanism, and the dislocation-driven and VLS nanowire growth mechanisms might coexist and compete with each other. Further investigation and understanding of the growth of these nanomaterials can allow for more controllable synthesis of various new 1D structured materials by enabling different growth mechanisms under selected synthesis conditions.

METHODS

CVD Synthesis of CdS and CdSe Nanowires. A tube furnace equipped with a 1-in. quartz tube (Thermal Fisher, Linderberg Blue M, model TF55030KC-1) connected to Ar and H_2 gas inlets and a vacuum pump was used as the reactor. Typically, 20 mg of $CdCl_2$, 60 mg of sulfur, or 60 mg of selenium powder was placed in different porcelain boats inside the quartz tube as solid reactants. The silicon/SiO_2 substrates (Nova Electronic Materials, p-type, 500 nm thermal oxide), covered with or without homemade gold nanoparticles (13 nm), were placed downstream of the furnace to collect the products. The system was pumped down to 0.1 Torr, flushed with argon flow (100 sccm) for a few cycles, and rapidly heated to the targeted temperature (*e.g.*, 600 °C). The porcelain boat containing sulfur or selenium powder was then inserted into the heating zone of the furnace, and H_2 was started to flow (25 sccm) as a reacting/carrier gas for 5–15 min, before the furnace was cooled to room temperature. The temperatures and pressured used for growth of different nanostructures are summarized in Table S1.

SEM and TEM Characterization. Substrates with deposited CdS or CdSe products were directly mounted onto metallic pucks for SEM imaging at 1 kV (Hitachi S4800) or 20 kV (Philips XL30).

For TEM and SAED analysis, growth substrates were sonicated in ethanol for 10 s to disperse the as-grown CdS or CdSe products. Then 10−50 μL of ethanol suspension was dropped onto a copper grid (Ted Pella Inc., Lacey Formvar/Carbon on 300 mesh copper grids, #01883-F). TEM and SAED analysis were carried out with either a Philips-CM200 or a JEOL-2100F microscope at an accelerating voltage of 200 kV.

X-ray Diffraction and Photoluminescence. X-ray diffraction data were collected on a Bruker SMART APEX (II)-CCD X-ray single-crystal diffractometer with Cu Kα radiation (λ = 1.5418 Å). For photoluminescence measurement, the substrates with CdS or CdSe products were first observed using an optical microscope (Olympus, BX51) under both the bright-field and the dark-field modes and then illumined by a mercury lamp. The photoluminescence spectra were collected by a spectrometer equipped with a charge-coupled device (PG2000 Pro, Idea Optics Co., Ltd., China).

Conflict of Interest: The authors declare no competing financial interest.

Acknowledgment. G.Z. thanks the NSF of China (21071033), the Program for New Century Excellent Talents in University (NCET-10-0357), the Program for Professor of Special Appointment (Eastern Scholar) at Shanghai Institutions of Higher Learning, and the Shanghai Pujiang Program (10PJ1401000). S.J., F.M., and L.L. thank the NSF (grant DMR-1106184), Research Corporation SciaLog Award, the Sloan Research Fellowship, and Honeywell University Affiliate Fund for support.

Supporting Information Available: Schematic illustration of experiment setup, table of synthesis conditions, SEM images of CdS nanowires grown without catalysts, TEM images of bend contour, twist contour, stacking faults, dislocation contrast, and tubular structures observed in various CdS/CdSe nanostructures. This material is available free of charge *via* the Internet at http://pubs.acs.org.

REFERENCES AND NOTES

1. Lieber, C. M.; Wang, Z. L. Functional Nanowires. *MRS Bull.* **2007**, *32*, 99–108.
2. Law, M.; Goldberger, J.; Yang, P. D. Semiconductor Nanowires and Nanotubes. *Annu. Rev. Mater. Res.* **2004**, *34*, 83–122.
3. Schmitt, A. L.; Higgins, J. M.; Szczech, J. R; Jin, S. Synthesis and Applications of Metal Silicide Nanowires. *J. Mater. Chem.* **2010**, *20*, 223–235.
4. Hochbaum, A. I.; Yang, P. Semiconductor Nanowires for Energy Conversion. *Chem. Rev.* **2009**, *110*, 527–546.
5. Yan, R.; Gargas, D.; Yang, P. Nanowire Photonics. *Nat. Photonics* **2009**, *3*, 569–576.
6. Tian, B.; Kempa, T. J.; Lieber, C. M. Single Nanowire Photovoltaics. *Chem. Soc. Rev.* **2009**, *38*, 16–24.
7. Lu, W.; Lieber, C. M. Nanoelectronics from the Bottom Up. *Nat. Mater.* **2007**, *6*, 841–850.
8. Wagner, R. S.; Ellis, W. C. Vapor-Liquid-Solid Mechanism of Single Crystal Growth. *Appl. Phys. Lett.* **1964**, *4*, 89–90.
9. Morales, A. M.; Lieber, C. M. A Laser Ablation Method for the Synthesis of Crystalline Semiconductor Nanowires. *Science* **1998**, *279*, 208–211.
10. Persson, A. I.; Larsson, M. W.; Stenström, S.; Ohlsson, B. J.; Samuelson, L.; Wallenberg, L. R. Solid-Phase Diffusion Mechanism for GaAs Nanowire Growth. *Nat. Mater.* **2004**, *3*, 677–681.
11. Lensch-Falk, J. L.; Hemesath, E. R.; Perea, D. E.; Lauhon, L. J. Alternative Catalysts for VSS Growth of Silicon and Germanium Nanowires. *J. Mater. Chem.* **2009**, *19*, 849–857.
12. Trentler, T. J.; Hickman, K. M.; Goel, S. C.; Viano, A. M.; Gibbons, P. C.; Buhro, W. E. Solution-Liquid-Solid Growth of Crystalline III-V Semiconductors: An Analogy to Vapor-Liquid-Solid Growth. *Science* **1995**, *270*, 1791–1794.
13. Wang, F.; Dong, A.; Sun, J.; Tang, R.; Yu, H.; Buhro, W. E. Solution-Liquid-Solid Growth of Semiconductor Nanowires. *Inorg. Chem.* **2006**, *45*, 7511–7521.
14. Bierman, M. J.; Lau, Y. K. A.; Kvit, A. V.; Schmitt, A. L.; Jin, S. Dislocation-Driven Nanowire Growth and Eshelby Twist. *Science* **2008**, *320*, 1060–1063.
15. Morin, S. A.; Bierman, M. J.; Tong, J.; Jin, S. Mechanism and Kinetics of Spontaneous Nanotube Growth Driven by Screw Dislocations. *Science* **2010**, *328*, 476–480.
16. Jin, S.; Bierman, M. J.; Morin, S. A. A New Twist on Nanowire Formation: Screw-Dislocation-Driven Growth of Nanowires and Nanotubes. *J. Phys. Chem. Lett.* **2010**, *1*, 1472–1480.
17. Markov, I. V. *Crystal Growth for Beginners: Fundamentals of Nucleation, Crystal Growth, and Epitaxy*, 1st ed.; World Scientific Publishing Co. Pte. Ltd.: Singapore, 1995.
18. Lau, Y. K. A.; Chernak, D. J.; Bierman, M. J.; Jin, S. Formation of PbS Nanowire Pine Trees Driven by Screw Dislocations. *J. Am. Chem. Soc.* **2009**, *131*, 16461–16471.
19. Zhu, J.; Peng, H. L.; Marshall, A. F.; Barnett, D. M.; Nix, W. D.; Cui, Y. Formation of Chiral Branched Nanowires by the Eshelby Twist. *Nat. Nanotechnol.* **2008**, *3*, 477–481.
20. Morin, S. A.; Jin, S. Screw Dislocation-Driven Epitaxial Solution Growth of ZnO Nanowires Seeded by Dislocations in GaN Substrates. *Nano Lett.* **2010**, *10*, 3459–3463.
21. Li, Y. G.; Wu, Y. Y. Critical Role of Screw Dislocation in the Growth of $Co(OH)_2$ Nanowires as Intermediates for Co_3O_4 Nanowire Growth. *Chem. Mater.* **2010**, *22*, 5537–5542.
22. Meng, F.; Morin, S. A.; Jin, S. Rational Solution Growth of α-FeOOH Nanowires Driven by Screw Dislocations and Their Conversion to α-Fe_2O_3 Nanowires. *J. Am. Chem. Soc.* **2011**, *133*, 8408–8411.
23. Meng, F.; Jin, S. The Solution Growth of Copper Nanowires and Nanotubes is Driven by Screw Dislocations. *Nano Lett.* **2012**, *12*, 234–239.
24. Hacialioglu, S.; Meng, F.; Jin, S. Facile Large-Scale Solution Synthesis of Cu_2O Nanowires and Nanotubes Driven by Screw Dislocations. *Chem. Commun.* **2012**, *48*, 1174–1176.
25. Bartolomé, J.; Maestre, D.; Amati, M.; Cremades, A.; Piqueras, J. Indium Zinc Oxide Pyramids with Pinholes and Nanopipes. *J. Phys. Chem. C* **2011**, *115*, 8354–8360.
26. Tizei, L. H. G.; Craven, A. J.; Zagonel, L. F.; Tencé, M.; Stéphan, O.; Chiaramonte, T.; Cotta, M. A.; Ugarte, D. Enhanced Eshelby Twist on Thin Wurtzite InP Nanowires and Measurement of Local Crystal Rotation. *Phys. Rev. Lett.* **2011**, *107*, 195503.
27. Maestre, D.; Haeussler, D.; Cremades, A.; Jaeger, W.; Piqueras, J. Complex Defect Structure in the Core of Sn-Doped In_2O_3 Nanorods and Its Relationship with a Dislocation-Driven Growth Mechanism. *J. Phys. Chem. C* **2011**, *115*, 18083–18087.
28. Maestre, D.; Haeussler, D.; Cremades, A.; Jaeger, W.; Piqueras, J. Nanopipes in In_2O_3 Nanorods Grown by a Thermal Treatment. *Cryst. Growth Des.* **2011**, *11*, 1117–1121.
29. Morin, S. A.; Forticaux, A.; Bierman, M. J.; Jin, S. Screw Dislocation-Driven Growth of Two-Dimensional Nanoplates. *Nano Lett.* **2011**, *11*, 4449–4455.
30. Chikawa, J.; Nakayama, T. Dislocation Structure and Growth Mechanism of Cadmium Sulfide Crystals. *J. Appl. Phys.* **1964**, *35*, 2493–2501.
31. Zhai, T.; Fang, X.; Li, L.; Bando, Y.; Golberg, D. One-Dimensional CdS Nanostructures: Synthesis, Properties, and Applications. *Nanoscale* **2010**, *2*, 168–187.
32. Huynh, W. U.; Dittmer, J. J.; Alivisatos, A. P. Hybrid Nanorod-Polymer Solar Cells. *Science* **2002**, *295*, 2425–2427.
33. Yu, Y. H.; Kamat, P. V.; Kuno, M. A CdSe Nanowire/Quantum Dot Hybrid Architecture for Improving Solar Cell Performance. *Adv. Funct. Mater.* **2010**, *20*, 1464–1472.
34. Kongkanand, A.; Tvrdy, K.; Takechi, K.; Kuno, M.; Kamat, P. V. Quantum Dot Solar Cells. Tuning Photoresponse Through Size and Shape Control of CdSe-TiO_2 Architecture. *J. Am. Chem. Soc.* **2008**, *130*, 4007–4015.
35. Wang, G. M.; Yang, X. Y.; Qian, F.; Zhang, J. Z.; Li, Y. Double-Sided CdS and CdSe Quantum Dot Co-Sensitized ZnO Nanowire Arrays for Photoelectrochemical Hydrogen Generation. *Nano Lett.* **2010**, *10*, 1088–1092.
36. Sun, W. T.; Yu, Y.; Pan, H. Y.; Gao, X. F.; Chen, Q.; Peng, L. M. CdS Quantum Dots Sensitized TiO_2 Nanotube-Array Photoelectrodes. *J. Am. Chem. Soc.* **2008**, *130*, 1124–1125.
37. Erwin, S. C.; Zu, L. J.; Haftel, M. I.; Efros, A. L.; Kennedy, T. A.; Norris, D. J. Doping Semiconductor Nanocrystals. *Nature* **2005**, *436*, 91–94.

38. Huang, Y.; Duan, X. F.; Lieber, C. M. Nanowires for Integrated Multicolor Nanophotonics. *Small* **2005**, *1*, 142–147.
39. Xie, R. G.; Kolb, U.; Li, J. X.; Basche, T.; Mews, A. Synthesis and Characterization of Highly Luminescent CdSe-Core $CdS/Zn_{0.5}Cd_{0.5}S/ZnS$ Multishell Nanocrystals. *J. Am. Chem. Soc.* **2005**, *127*, 7480–7488.
40. Cho, C.-H.; Aspetti, C. O.; Turk, M. E.; Kikkawa, J. M.; Nam, S.-W.; Agarwal, R. Tailoring Hot-Exciton Emission and Lifetimes in Semiconducting Nanowires *via* Whispering-Gallery Nanocavity Plasmons. *Nat. Mater.* **2011**, *10*, 669–675.
41. Greytak, A. B.; Barrelet, C. J.; Li, Y.; Lieber, C. M. Semiconductor Nanowire Laser and Nanowire Waveguide Electro-Optic Modulators. *Appl. Phys. Lett.* **2005**, *87*, 151103.
42. Agarwal, R.; Barrelet, C. J.; Lieber, C. M. Lasing in Single Cadmium Sulfide Nanowire Optical Cavities. *Nano Lett.* **2005**, *5*, 917–920.
43. Pan, A.; Zhou, W.; Leong, E. S. P.; Liu, R.; Chin, A. H.; Zou, B.; Ning, C. Z. Continuous Alloy-Composition Spatial Grading and Superbroad Wavelength-Tunable Nanowire Lasers on a Single Chip. *Nano Lett.* **2009**, *9*, 784–788.
44. Piccione, B.; van Vugt, L. K.; Agarwal, R. Propagation Loss Spectroscopy on Single Nanowire Active Waveguides. *Nano Lett.* **2010**, *10*, 2251–2256.
45. van Vugt, L. K.; Piccione, B.; Cho, C. H.; Aspetti, C.; Wirshba, A. D.; Agarwal, R. Variable Temperature Spectroscopy of As-Grown and Passivated CdS Nanowire Optical Waveguide Cavities. *J. Phys. Chem. A* **2011**, *115*, 3827–3833.
46. Ma, R. M.; Dai, L.; Huo, H. B.; Xu, W. J.; Oin, G. G. High-Performance Logic Circuits Constructed on Single CdS Nanowires. *Nano Lett.* **2007**, *7*, 3300–3304.
47. Zhang, Y.; Tang, Y.; Lee, K.; Ouyang, M. Catalytic and Catalyst-Free Synthesis of CdSe Nanostructures with Single-Source Molecular Precursor and Related Device Application. *Nano Lett.* **2008**, *9*, 437–441.
48. Grebinski, J. W.; Hull, K. L.; Zhang, J.; Kosel, T. H.; Kuno, M. Solution-Based Straight and Branched CdSe Nanowires. *Chem. Mater.* **2004**, *16*, 5260–5272.
49. Yu, Y.; Kamat, P. V.; Kuno, M. A CdSe Nanowire/Quantum Dot Hybrid Architecture for Improving Solar Cell Performance. *Adv. Funct. Mater.* **2010**, *20*, 1464–1472.
50. Xu, D. S.; Shi, X. S.; Guo, G. L.; Gui, L. L.; Tang, Y. Q. Electrochemical Preparation of CdSe Nanowire Arrays. *J. Phys. Chem. B* **2000**, *104*, 5061–5063.
51. Routkevitch, D.; Bigioni, T.; Moskovits, M.; Xu, J. M. Electrochemical Fabrication of CdS Nanowire Arrays in Porous Anodic Aluminum Oxide Templates. *J. Phys. Chem.* **1996**, *100*, 14037–14047.
52. Ma, C.; Ding, Y.; Moore, D.; Wang, X. D.; Wang, Z. L. Single-Crystal CdSe Nanosaws. *J. Am. Chem. Soc.* **2004**, *126*, 708–709.
53. Wang, Y. W.; Meng, G. W.; Zhang, L. D.; Liang, C. H.; Zhang, J. Catalytic Growth of Large-Scale Single-Crystal CdS Nanowires by Physical Evaporation and Their Photoluminescence. *Chem. Mater.* **2002**, *14*, 1773–1777.
54. Utama, M. I. B.; Peng, Z.; Chen, R.; Peng, B.; Xu, X.; Dong, Y.; Wong, L. M.; Wang, S.; Sun, H.; Xiong, Q. Vertically Aligned Cadmium Chalcogenide Nanowire Arrays on Muscovite Mica: A Demonstration of Epitaxial Growth Strategy. *Nano Lett.* **2010**, *11*, 3051–3057.
55. Pan, A.; Liu, R.; Sun, M.; Ning, C. Z. Quaternary Alloy Semiconductor Nanobelts with Bandgap Spanning the Entire Visible Spectrum. *J. Am. Chem. Soc.* **2009**, *131*, 9502–9503.
56. Ge, J. P.; Li, Y. D. Selective Atmospheric Pressure Chemical Vapor Deposition Route to CdS Arrays, Nanowires, and Nanocombs. *Adv. Funct. Mater.* **2004**, *14*, 157–162.
57. Barrelet, C. J.; Wu, Y.; Bell, D. C.; Lieber, C. M. Synthesis of CdS and ZnS Nanowires Using Single-Source Molecular Precursors. *J. Am. Chem. Soc.* **2003**, *125*, 11498–11499.
58. Zheng, J.; Song, X. B.; Chen, N.; Li, X. G. Highly Symmetrical CdS Tetrahedral Nanocrystals Prepared by Low-Temperature Chemical Vapor Deposition Using Polysulfide as the Sulfur Source. *Cryst. Growth Des.* **2008**, *8*, 1760–1765.
59. Jung, Y.; Ko, D.-K.; Agarwal, R. Synthesis and Structural Characterization of Single-Crystalline Branched Nanowire Heterostructures. *Nano Lett.* **2006**, *7*, 264–268.
60. Lee, S. K. C.; Yu, Y.; Perez, O.; Puscas, S.; Kosel, T. H.; Kuno, M. Bismuth-Assisted CdSe and CdTe Nanowire Growth on Plastics. *Chem. Mater.* **2009**, *22*, 77–84.
61. Bierman, M. J.; Lau, Y. K. A.; Jin, S. Hyperbranched PbS and PbSe Nanowires and the Effect of Hydrogen Gas on Their Synthesis. *Nano Lett.* **2007**, *7*, 2907–2912.
62. Manna, L.; Milliron, D. J.; Meisel, A.; Scher, E. C.; Alivisatos, A. P. Controlled Growth of Tetrapod-Branched Inorganic Nanocrystals. *Nat. Mater.* **2003**, *2*, 382–385.
63. Utama, M. I. B.; Zhang, Q.; Jia, S.; Li, D.; Wang, J.; Xiong, Q. Epitaxial II–VI Tripod Nanocrystals: A Generalization of van der Waals Epitaxy for Nonplanar Polytypic Nanoarchitectures. *ACS Nano* **2012**, *6*, 2281–2288.
64. Williams, D. B.; Carter, C. B. *Transmission Electron Microscopy: a Textbook for Materials Science*, 1st ed.; Plenum Press: New York, 1996.
65. Hall, D.; Baeon, D. J. *Introduction to Dislocations*, 4th ed.; Pergamon: Oxford, 2001.
66. Eshelby, J. D. Screw Dislocations in Thin Rods. *J. Appl. Phys.* **1953**, *24*, 176–179.
67. Eshelby, J. D. The Twist in a Crystal Whisker Containing a Dislocation. *Philos. Mag.* **1958**, *3*, 440–447.
68. Zhang, D. B.; Akatyeva, E.; Dumitrică, T. Helical BN and ZnO Nanotubes with Intrinsic Twisting: An Objective Molecular Dynamics Study. *Phys. Rev. B* **2011**, *84*, 115431.
69. Nikiforov, I.; Zhang, D. B.; Dumitrică, T. Screw Dislocations in ⟨100⟩ Silicon Nanowires: An Objective Molecular Dynamics Study. *J. Phys. Chem. Lett.* **2011**, *2*, 2544–2548.
70. Shan, C. X.; Liu, Z.; Hark, S. K. CdSe Nanowires with Controllable Growth Orientations. *Appl. Phys. Lett.* **2007**, *90*, 193123.